Letter

Poly[2,5-bis(3-dodecylthiophen-2-yl)thieno[3,2-b]thiophene] Oligomer Single-Crystal Nanowires from Supercritical Solution and their Anisotropic Exciton Dynamics

Nicholas S Colella, Joelle A. Labastide, Benjamin P Cherniawski, Hilary B. Thompson, Sarah R Marques, Lei Zhang, Özlem Usluer, James J. Watkins, Alejandro L. Briseno, and Michael D. Barnes

Just Accepted

Poly[2,5-bis(3-dodecylthiophen-2-yl)thieno[3,2-b]thiophene] Oligomer Single-Crystal Nanowires from Supercritical Solution and their Anisotropic Exciton Dynamics

Nicholas S. Colella[1#+], Joelle A. Labastide[2*#], Benjamin P. Cherniawski[1], Hilary B. Thompson[2], Sarah R. Marques[2], Lei Zhang[1], Özlem Usluer[1,2,3], James J. Watkins,[1] Alejandro L. Briseno[1**], and Michael D. Barnes[2,4**]

Department of Polymer Science of Engineering[1], Department of Chemistry[2], *Department of Energy System Engineering, Necmettin Erbakan University, 42000, Konya, Turkey*[3], Department of Physics[4] University of Massachusetts Amherst

*current address: Dept. of Physics, University of Massachusetts Amherst
+ current address: Dept. of Chemistry and Chemical Biology, Harvard University
# authors contributed equally to this work
** Email: abriseno@mail.pse.umass.edu; mdbarnes@chem.umass.edu

Abstract

Supercritical fluids, exhibiting a combination of liquid-like solvation power and gas-like diffusivity, are a relatively unexplored medium for processing and crystallization of oligomer and polymeric semiconductors whose opto-electronic properties critically depend on the microstructure. Here we report oligomer crystallization from the polymer organic semiconductor, poly[2,5-bis(3-dodecylthiophen-2-yl)thieno[3,2-b]thiophene] (PBTTT) in supercritical hexane, yielding needle-like single crystals up to several microns in length. We characterize the crystals photo-physical properties by time- and polarization-resolved photoluminescence (TPRPL) spectroscopy. These techniques reveal two-dimensional inter-chromophore coupling facilitated by the high degree of π-stacking order within the crystal. Furthermore, the crystals obtained from supercritical fluid were found to be similar photophysically as the crystallites found in solution-cast thin films, and distinct from solution-grown crystals which exhibited spectroscopic signatures indicative of different packing geometries.

The promise of low-cost, solution-processable organic optoelectronics has driven an enormous research effort in areas of organic photovoltaics, field-effect transistors, sensors, and a host of other practical devices.[1-13] While organic semiconductors can be inexpensively processed from solution, their solid-state morphology, and therefore device performance, is largely dependent on processing conditions.[14-19] For example, it is well known that defects in assemblies – even in very low concentrations – can seriously impede exciton and/or charge transport. [20, 21] Single crystal nanowires represent a desirable platform for characterizing optoelectronic interactions in these promising materials due to their high purity and exceptionally low conformational entropy.[22-26] Single crystals of organic semiconductors are well-known to have emergent properties that are distinct from their single-molecule or amorphous film counterparts.[2, 27-32] Band-like transport and the Hall effect, for example, have been revealed in single-crystals of p-type rubrene[31, 33] and n-type perylene diimide (PDIF-CN$_2$).[34] Additionally, the photo-physics of rubrene single crystals have been explored, revealing the roles of traps and electron-phonon interactions on charge carrier dynamics,[35, 36] as well as anisotropic exciton diffusion.[37] In particular, *directional* inter-chromophore electronic coupling – which mediate exciton transport and intrinsic charge separation - are not only experimentally accessible solely in crystals, but also are highly sensitive to packing geometry.[38-40]

Single crystals are accessible through a several techniques (e.g. physical vapor transport (PVT), solution evaporation, and solvent/anti-solvent crystallization) however the material limitations often preclude certain crystallization strategies. In general, techniques for creating semiconductor single crystals have been largely limited to a small class of organic materials that undergo self-assembly in marginal solvents. Additionally, polymorphism has been reported in materials undergoing different crystallization conditions.[41] This motivates development and exploration of new crystallization strategies for organic semiconductors in order to provide opportunities for crystallization of previously non-processable materials and to provide a handle to access new crystalline polymorphs.

In this Letter, we demonstrate an approach to crystallize organic semiconductors based on supercritical fluids and show that poly[2,5-bis(3-dodecylthiophen-2-yl)thieno[3,2-b]thiophene] (PBTTT) oligomers in supercritical hexane form needle-like single-crystals up to several hundred microns in length. Supercritical fluids (SCFs), having both gas-like and liquid-like properties, represent an interesting and largely unexplored solvent medium for the crystallization of a variety of material solutes.[42] The properties of SCFs are readily modulated by temperature and pressure of the solvent, which allows for a well-controlled and tunable crystallization environment. The work reported herein represents the first time that SCFs have been used to crystallize organic semiconductors. Additionally, polarized optical interrogation of isolated PBTTT crystals showed spectroscopic hallmarks of strong Frenkel exciton coupling and inter-chain charge-transfer that manifest in highly anisotropic exciton dynamics. Most notably, these

SCF crystals show different photo-physical behavior as compared to their counterparts made by slow evaporation of solvent. Notably, the crystals formed via the SCF process exhibit photophysical properties analogous to those observed for the crystallites of the thin film, while solution-grown crystals display a spectroscopic signature which is distinct from that observed of the thin-film crystallites. Thus, crystallization in SCFs alleviates the kinetic limitations of solution crystallization, resulting in the crystal polymorph which is most thermodynamically favorable.

To explore this technique and demonstrate its application to organic semiconductors, we examined a sample of poly[2,5-bis(3-dodecylthiophen-2-yl)thieno[3,2-b]thiophene] (PBTTT) (purchased from Luminescence Technology Corp.) in supercritical hexane (scHex). 5 mg of PBTTT with a high polydispersity index (PDI=3.60, as characterized by gel permeation chromatography (GPC) vs. polystyrene standards) was placed in an aluminum foil boat in a ~10 mL stainless steel high-pressure vessel which was charged with ~9 mL hexane. The area around the sample was heated to 290 °C and concurrently pressurized to 900 PSI ($T_{c,hexane}$ = 234.5 °C, $P_{c,hexane}$ = 438 PSI), resulting in a solvent density of 0.27 g/mL (see Supporting Information for temperature profile of the vessel).

Figure 1 shows (a) a schematic of the reactor, (b) the structure of PBTTT, and (c) a representative image of PBTTT crystals grown from scHex. Crystals ~200 nm wide and ~50 μm long were observed. These crystals were formed by the dissolution and diffusion of the molecules millimeters from the source material, where they nucleated on the rough aluminum surface and continued to grow into one-dimensional needle-like crystals. The average crystal width

Figure 1. (A) Stainless steel supercritical reactor with rope heater. The cross configuration, clockwise from the 12 o'clock position, consists of a pressure release valve, a pressure gauge, the lower end of which is wrapped with a rope heater, and a safety rupture disc assembly. Total internal volume is approximately 10 mL. (B) Molecular structure of PBTTT and BTTT1.5 (n=1). (C) Optical micrograph of the as-grown crystals.

was determined to be 196 ± 72 nm (see Supporting Information). This growth was insensitive to the reactor geometry; the hot zone containing the aluminum boat could be located at the top or
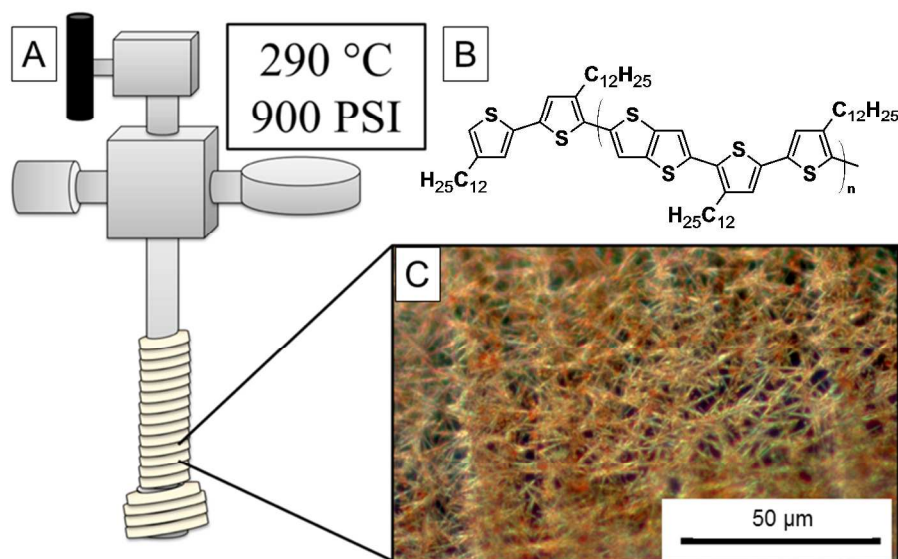
bottom of the steel cylinder. Due to the relatively aggressive solvent properties of scHex, syringe pumps could not be used to precisely modulate the pressure of the system; the amount of hexane loaded into the reactor prior to sealing and heating dictated the resulting pressure. The crystallization was found to be more dependent on the density of the supercritical fluid than the temperature, with crystals being formed with hot zones ranging from 250 – 320 °C, provided that the density was greater than ~0.3 g/ml (obtained at pressures greater than 600 – 1200 PSI, respectively).

Figure 2 also shows the optical (OM, A), atomic force (AFM, B, C), and transmission electron microscopy (TEM, E) and selected area electron diffraction (SAED, F) images of scHex crystals. The optical images reveal a network of large crystals, 20-50 μm in length, grown on the aluminum foil boat (Figure 1) and transferred to a polydimethylsiloxane (PDMS) stamp (Figure 2a). The images of these crystals are diffraction limited in the direction transverse to the crystal axis, and therefore their widths appear substantially larger under OM than their true dimensions as observed by AFM, SEM, and TEM. The crystals are hexagonal in cross-section, as

Figure 2. (A) Darkfield optical micrograph of crystals transferred to a PDMS stamp. (B) AFM phase image of a crystal stamped onto SiO2 (100° dynamic range). (C) Corresponding AFM height image and profile (inset). (D) MALDI-ToF of crystals and source material. (E) TEM micrograph of a single crystal. (F) Corresponding selected area electron diffraction pattern.

shown in Figures 2B-D. From the SAED, the unit cell parameters B, C, and α were determined to be 8.78 Å, 20.1 Å, and 90°, respectively.

Matrix-assisted laser desorption/ionization time-of-flight (MALDI-ToF) was employed to elucidate the molecular weight of the crystalized species (Figure 2D). Analysis of the mass spectra revealed that the crystals consisted of only one species with m/z = 1137 which represented the BTTT monomer with an additional bithiophene group (referred to herein as BTTT1.5). PBTTT is synthesized from a condensation polymerization of functionalized thienothiophene and bithiophene co-monomers which produces BTTT 1.5 oligomers in low conversion. The high PDI and low Mn of this source affords a significant population of BTTT1.5 for SCF crystallization. To help verify this material, we separately synthesized BTTT1.5, detailed synthesis is available in SI. Fractionation of aliphatic polymers in supercritical fluid has previously been reported,(43, 44) but this result is the first to show the fractionation and concurrent crystallization of conjugated materials.
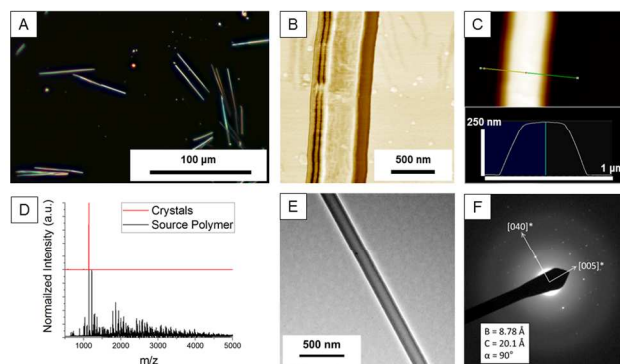
Figure 3 shows photoluminescence (PL) spectra of BTTT1.5 crystals formed in scHex compared with pure BTTT1.5 (synthesized via Stille coupling) in solution and crystallized from slow evaporation of hexanes at room temperature. The BTTT1.5 crystals formed *via* slow evaporations of hexanes were strongly red-shifted ($\approx$ 0.4 eV) compared to the PL origin observed for the solution and semicrystalline film and thus are not a good medium for determining the physics of charge transport in BTTT1.5 crystallites. Interestingly, the PBTTT

Figure 3. Wavelength resolved photoluminescence (following laser excitation at 488 nm) from pure BTTT1.5 in solution (blue diamonds), scHex-formed crystals (green pentagons), and crystallized from hexane solution (red squares). For comparison, the spin-cast PBTTT film spectrum is shown (grey pentagons).

crystals grown from supercritical fluid exhibited a spectral response that was very similar to the semicrystalline BTTT1.5 film, indicating that the crystal packing is representative of the polymorph most commonly observed in semicrystalline films used for thin film devices. Therefore, crystals obtained via crystallization in supercritical hexane are superior models for determining the intrinsic charge transport photophysics of BTTT1.5. The PL spectrum of the semicrystalline film was ostensibly equivalent to the crystals grown in supercritical hexane with a small additional contribution of high-energy emission that can be ascribed to the presence of some amorphous material in the film and marginally larger linewidths which are likely a result of intrinsic disorder in the film.

Figure 4. Excitation polarization analysis of PBTTT isolated crystals. (A) Representative photoluminescence intensity (open circles) and fit (solid blue line, $I = A\cos^2(b\theta + \phi)$) vs. excitation polarization orientation (dashed red line) referenced to crystal long-axis. (B) Representative PBTTT nanowire photoluminescence image and schematic indicating the optically relevant orientations of the crystal growth axis (Ca), transverse crystal axis (TCa), the chromophores (Ch), oriented at an angle ϕ = 25° ± 3 with respect to the axis transverse to the crystal growth axis.

Excitation polarization anisotropy experiments were performed on single scHex BTTT1.5 crystals by measuring the PL intensity as a function of linear excitation polarization orientation with respect to the crystal long axis (Ca). Figure 4 (A) shows the PL intensity response to the rotating linear polarization (blue circles), and the fit (solid blue line, $I = A\cos^2(b\theta + \phi)$), with the reference
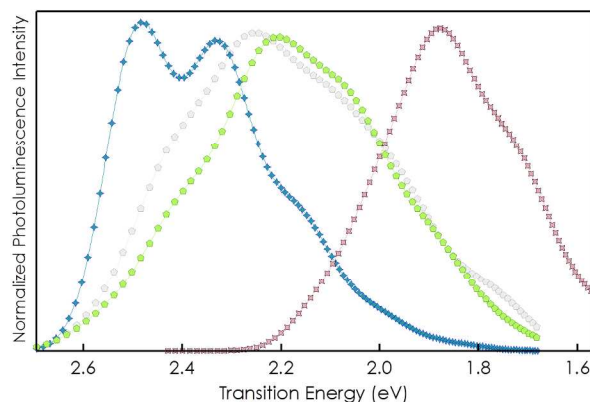
curve indicating the input polarization angle (dashed red line). The phase shift between maximum fluorescence response and crystal long axis gives the approximate orientation of the transition dipole moment within the crystal structure. Figure 4 (B) shows a representative PL image and crystal schematic with crystal axis (Ca) and transverse crystal axis (TCa) indicated in yellow. The phase shift ($\phi = 25°$) indicated the orientation of the conjugated BTTT1.5 backbones with respect to the TCa obtained from the fit to excitation polarization anisotropy measurements; this orientation was designated the chromophore axis (Ch) and is indicated on the schematic in light blue. This chromophore angle determined from the polarization phase shift (ϕ) extracted from polarization measurements constitutes a complementary monoclinic angle of 62-68°, which is consistent with similar oligomeric crystals.(45) The uncertainty ($\pm 3°$) in the phase angle represents a one standard deviation from a distribution of values obtained from surveying over 80 single crystals from different batches, indicating that the crystallization method presented here reliably yields crystals with virtually identical internal structure.

The large modulation depth associated with the excitation polarization, ($M = \frac{I_{max}-I_{min}}{I_{max}+I_{min}}$), indicates a high degree of chromophore alignment within the structure, as 80% of the total oscillator strength appears along the chromophore axis (Ch). While it might be anticipated that an ideal single crystal should show a polarization contrast approaching unity (M=1) (indicating that all chromophores are aligned along the same axis), there is a growing body of evidence that suggests that charge-transfer interactions that act primarily along the π-stacking axis give rise to an optical transition moment essentially perpendicular to the chromophore axis.(38, 46, 47) In the HJ-aggregate model of chromophore interactions in crystalline assemblies of organic semiconductors, the usual Holstein Hamiltonian (describing long-range Coulombic dipole-dipole interactions) is augmented with a charge-transfer (CT) component as well as a coupling between diabatic Coulombic and CT interactions whose sign and magnitude are sensitive to sub-Å molecular displacements in packing.(47, 48) We propose that it is this mixing of diabatic Frenkel exciton (Coulombic) and CT states that gives rise to a two-dimensional transition moment and associated polarization mixing in photoluminescence that has been observed in P3HT nanofibers(26) and tetraazaterrylene (TAT) nanowire crystals.(38) In these systems, time- and polarization-resolved photoluminescence (TPRPL) revealed emission polarized parallel to the fiber growth axis (perpendicular to the polymer chain axis) corresponding to recombination of inter-chain excitons. The influence of CT interactions on work-function modification in P3HT assemblies with varying inter-chain coupling strength has recently been observed.(49) More recently, similar observations have been made in crystalline assemblies of tetraazaterrylene (TAT), where we have reported similar 2-dimensional polarization dynamics and directional charge-separation which is a manifestation of a strong (≈ 150 meV) inter-chromophore CT interaction. The presence of a reasonably strong inter-chain transition dipole moment (as evidenced by the polarization anisotropy) puts BTTT1.5 single crystals in a small class of two-dimensionally absorbing polymeric materials and has important consequences regarding its charge separation and transport processes.

We used time- and polarization-resolved photoluminescence (TPRPL) to probe the time-dependent mixing of polarization and the dependence on excitation polarization orientation with respect to the crystal axis. In this experiment, an isolated nanowire is selected and oriented in the x-y laboratory plane such that the crystal long axis is aligned along a single polarization channel in the detection setup. A pair of avalanche photodiodes arranged in a Hanbury Brown-Twiss configuration detect the arrival time and polarization (parallel or perpendicular with respect to the crystal long axis) of the PL photons. The signals in each polarization channel were then binned to construct a time-trajectory of the polarization contrast, M(t), defined as [N_{para}(t + Δt) - N_{perp}(t + Δt)]/[N_{para}(t + Δt) + N_{perp}(t + Δt)]. We chose a non-linear time-binning so that approximately equal total numbers of photons were collected in each bin, giving a uniform uncertainty in M(t).

Figure 5 (B-E) shows the typical results of TPRPL experiments conducted on isolated scHex BTTT1.5 single-crystals with 4 different excitation polarization orientations. In this measurement scheme, both arrival time and polarization state of detected
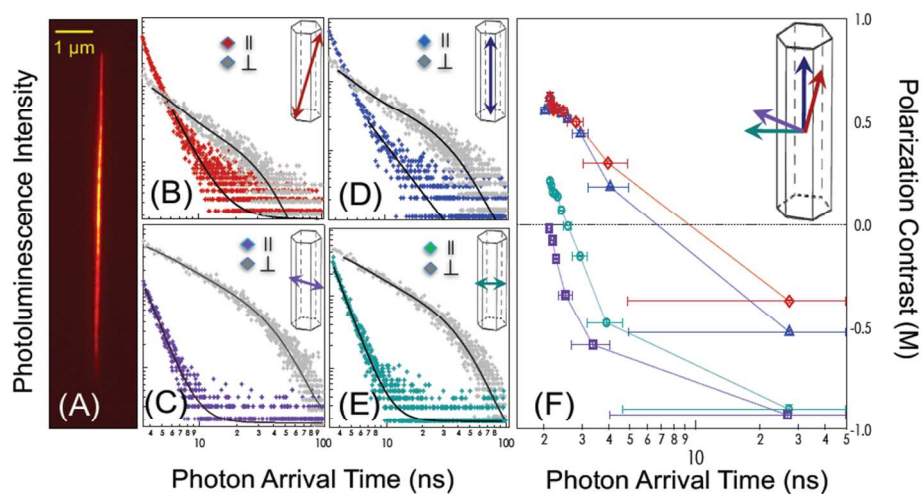

Figure 5. Time and polarization resolved photoluminescence from single PBTTT oligomer crystals. Representative PL image (A) with 4-axis excitation polarization orientations indicated by colored arrows corresponding to the crystal axis (Ca, blue), transverse crystal axis (TCa, green), chromophore axis (Ch, purple) and transverse chromophore axis (TCh, red). Photoluminescence decay curves (B-E) resolved into components polarized along Ca (in color) and TCa (in grey) from the same crystal, excited along each of the 4 axes, showing power law fits to the Ca emission and exponential fits to the TCA emission. (F): The time resolved polarization contrast parameter for excitation along each of the 4 axes.

photoluminescence photons are measured for linearly polarized excitation pulses with four different fixed orientations with respect to the crystal long-axis: The crystal axis (Ca, blue), the transverse crystal axis (TCa, green), the chromophore axis (Ch, purple) and the transverse chromophore axis (TCh, red) corresponding to the arrows superimposed on the crystal schematic in (F). After excitation, photoluminescence decay (B-E) is resolved into orthogonal polarization components corresponding to the crystal (Ca, colour) and transverse crystal (TCa, grey) axes. The photoluminescence decay is direction-specific in all cases, showing exponential decay ($I(t) = \sum_n A_n e^{-t/\tau_n}$) dynamics characteristic of bound-exciton recombination for TCa-polarized emission, and power law decays ($I(t) = At^{-p}$) characteristic of polaron pair recombination for Ca-polarized emission.

The presence of power law decay dynamics, and their association with emission events along the π-stack, suggests a strong contribution from a charge transfer mechanism mediated by the tightly packed, cofacial alignment of chromophores inside the crystal.(38, 50, 51) We also observed significantly smaller power law exponents (p~2.8) when exciting along the crystal (5D) and transverse chromophore (5C) axes, compared to the other two excitation directions (where p~3.7), potentially indicative of *larger* electron-hole separation distances achieved by directly activating the charge transfer mechanism.

The TPRPL measurements (5F) probe the (directional) fate of excitons within the crystal as a function of excited state lifetime, as a response to excitation polarization, which influences branching ratios for excitonic or charge-separated species along different crystallographic axes. We define the time-dependent polarization contrast, $M(\tau) = \frac{I_{CA}(\tau) - I_{TCA}(\tau)}{I_{CA}(\tau) + I_{TCA}(\tau)}$, thus *positive* /*negative* values of $M(\tau)$ correspond to emission polarized predominantly *parallel* and *transverse* to the crystal axis, respectively. When excited transverse to the crystal axis, there is a moderate initial emission anisotropy ($M(\tau=0)=0.3$), which decays quickly to a very large, negative final value ($M(\tau \sim 50$ ns$)= -0.9$). Excitation along the chromophore axis yields an essentially unpolarized initial state ($M(\tau =0)=0$) which decays to the same strongly polarized final state. Excitations along the crystal and the transverse chromophore axes have nearly identical evolutions, having initial emission polarized relatively strongly along the crystal axis ($M(\tau =0)=0.6$), and decaying to a moderate final value of ~ -0.45.

There are several remarkable qualities of BTTT1.5 crystals that are revealed by the time-resolved polarization anisotropy measurements. The first is that the excitation polarization strongly influences the fate of photo-generated excitations, illustrating the two-dimensional chromophore coupling within the crystal. Most noteworthy are the *positive* M values near t = 0, which indicate that excitation along the pi-stacking axis will preferentially populate inter-chromophore states. This phenomenon has never been seen in crystalline polymer assemblies, and we believe it to be a unique feature of H-aggregates. Secondly, the small, slightly positive values of the polarization contrast occurring in response to transverse or chromophore axis excitation suggest that the charge transfer mechanism is fast relative to the excitonic radiative lifetime. The observation of remarkably long-lived excitons polarized transverse to the crystal axis (as signaled by exponential decay constants between 16 and 19 ns) and preferentially generated upon chromophore and transverse crystal axis excitation is interesting, and serves as a likely explanation for the largely negative final values of M. The longevity of these excitations creates a possibility of very long diffusion lengths, which may obviate problematic design constraints for donor-acceptor interface engineering in active layers. Hole traps located at the boundaries between crystal facets may be responsible for the long-lived excitons polarized transverse to the crystal axis, and may function as charge-injection sites which ultimately enhance charge separation mechanics by reducing radiative recombination rates significantly.

In summary, we report the fractionation and crystallization of a polydisperse PBTTT source using supercritical hexane to yield virtually perfect, microscale single crystals of oligomeric BTTT1.5 with promising photophysical properties. This novel crystallization method leverages the solubilizing and transport properties of supercritical fluids to create a system that combines the advantages of crystallizations from vapor and solution and could be broadly applied to the crystallization of other organic semiconducting systems. The internal structure of the hexagonal PBTTT oligomer crystals produced in this study were probed via TEM and polarized photoluminescence measurements, revealing strongly coupled chromophores that are oriented 25° relative to the transverse crystal axis. The close packing and cofacial chromophore alignment within the crystal structure result in fast charge transfer and exciton separation along the π-stack, as well as long-lived excitons that may have very long diffusion lengths and are confined to the transverse crystal axis. The single crystal platform afforded a unique opportunity to investigate the potential presence of two-dimensional electronic coupling and polarization-anisotropic photophysical response to excitation, using 4-angle TPRPL experiments. Further studies into the H-aggregate nature of these crystals, as well as their potential for single crystal optoelectronic devices, are currently underway.

References.

(1)   Darling, S. B.; You, F. The Case for Organic Photovoltaics. *RSC Adv.* **2013**, *3* (39), 17633–17648.

(2)   Hasegawa, T.; Takeya, J. Organic Field-Effect Transistors Using Single Crystals. *Sci. Technol. Adv. Mater.* **2009**, *10* (2), 24314.

(3)   Baeg, K.-J.; Caironi, M.; Noh, Y.-Y. Toward Printed Integrated Circuits Based on Unipolar or Ambipolar Polymer Semiconductors. *Adv. Mater.* **2013**, *25* (31), 4210–4244.

(4)   Briseno, A. L.; Mannsfeld, S. C. B.; Ling, M. M.; Liu, S.; Tseng, R. J.; Reese, C.; Roberts, M. E.; Yang, Y.; Wudl, F.; Bao, Z. Patterning Organic Single-Crystal Transistor Arrays. *Nature* **2006**, *444* (7121), 913–917.

(5)   Zaumseil, J. P3HT and Other Polythiophene Field-Effect Transistors. In *P3HT Revisited – From Molecular Scale to Solar Cell Devices*; Ludwigs, S., Ed.; Springer Berlin Heidelberg, 2014; pp 107–137.

(6)   Sirringhaus, H. Device Physics of Solution-Processed Organic Field-Effect Transistors. *Adv. Mater.* **2005**, *17* (20), 2411–2425.

(7)   Miao, Q. Ten Years of N-Heteropentacenes as Semiconductors for Organic Thin-Film Transistors. *Adv. Mater.* **2014**, *26* (31), 5541–5549.

(8)   Wei, Q.; Tajima, K.; Hashimoto, K. Bilayer Ambipolar Organic Thin-Film Transistors and Inverters Prepared by the Contact-Film-Transfer Method. *ACS Appl. Mater. Interfaces* **2009**, *1* (9), 1865–1868.

(9)   Facchetti, A. π-Conjugated Polymers for Organic Electronics and Photovoltaic Cell Applications. *Chem. Mater.* **2011**, *23* (3), 733–758.

(10)   Dou, L.; You, J.; Hong, Z.; Xu, Z.; Li, G.; Street, R. A.; Yang, Y. 25th Anniversary Article: A Decade of Organic/Polymeric Photovoltaic Research. *Adv. Mater.* **2013**, *25* (46), 6642–6671.

(11)   Forrest, S. R. The Path to Ubiquitous and Low-Cost Organic Electronic Appliances on Plastic. *Nature* **2004**, *428* (6986), 911–918.

(12)   Zhang, Y.; Dong, H.; Tang, Q.; Ferdous, S.; Liu, F.; Mannsfeld, S. C. B.; Hu, W.; Briseno, A. L. Organic Single-Crystalline P-N Junction Nanoribbons. *J. Am. Chem. Soc.* **2010**, *132* (33), 11580–11584.

(13)   Dong, H.; Fu, X.; Liu, J.; Wang, Z.; Hu, W. 25th Anniversary Article: Key Points for High-Mobility Organic Field-Effect Transistors. *Adv. Mater.* **2013**, *25* (43), 6158–6183.

(14)   Brady, M. A.; Su, G. M.; Chabinyc, M. L. Recent Progress in the Morphology of Bulk Heterojunction Photovoltaics. *Soft Matter* **2011**, *7* (23), 11065–11077.

(15)   Perez, L. A.; Rogers, J. T.; Brady, M. A.; Sun, Y.; Welch, G. C.; Schmidt, K.; Toney, M. F.; Jinnai, H.; Heeger, A. J.; Chabinyc, M. L.; et al. The Role of Solvent Additive Processing in High Performance Small Molecule Solar Cells. *Chem. Mater.* **2014**, *26* (22), 6531–6541.

(16)   Podzorov, V.; Menard, E.; Borissov, A.; Kiryukhin, V.; Rogers, J. A.; Gershenson, M. E. Intrinsic Charge Transport on the Surface of Organic Semiconductors. *Phys. Rev. Lett.* **2004**, *93* (8), 86602.

(17)   Noriega, R.; Rivnay, J.; Vandewal, K.; Koch, F. P. V; Stingelin, N.; Smith, P.; Toney, M. F.; Salleo, A. A General Relationship between Disorder, Aggregation and Charge Transport in Conjugated Polymers. *Nat. Mater.* **2013**, *12* (11), 1038–1044.

(18)   Mollinger, S. A.; Krajina, B. A.; Noriega, R.; Salleo, A.; Spakowitz, A. J. Percolation, Tie-Molecules, and the Microstructural Determinants of Charge Transport in Semicrystalline Conjugated Polymers. *ACS Macro Lett.* **2015**, 708–712.

(19)   Verilhac, J. M.; LeBlevennec, G.; Djurado, D.; Rieutord, F.; Chouiki, M.; Travers, J. P.;

1
2
3
4
5
6
7

Pron, A. Effect of Macromolecular Parameters and Processing Conditions on Supramolecular Organisation, Morphology and Electrical Transport Properties in Thin Layers of Regioregular poly(3-Hexylthiophene). *Synth. Met.* **2006**, *156*, 815–823.

8
9
10
11
12

(20)   Mikhnenko, O. V.; Kuik, M.; Lin, J.; Van Der Kaap, N.; Nguyen, T. Q.; Blom, P. W. M. Trap-Limited Exciton Diffusion in Organic Semiconductors. *Adv. Mater.* **2014**, *26* (12), 1912–1917.

13
14
15
16
17
18

(21)   Reid, O. G.; Rayermann, G. E.; Coffey, D. C.; Ginger, D. S. Imaging Local Trap Formation in Conjugated Polymer Solar Cells: A Comparison of Time-Resolved Electrostatic Force Microscopy and Scanning Kelvin Probe Imaging. *J. Phys. Chem. C* **2010**, *114* (48), 20672–20677.

19
20
21
22
23

(22)   Briseno, A. L.; Mannsfeld, S. C. B.; Lu, X.; Xiong, Y.; Jenekhe, S. a; Bao, Z.; Xia, Y. Fabrication of Field-Effect Transistors from Hexathiapentacene Single-Crystal Nanowires. *Nano Lett.* **2007**, *7* (3), 668–675.

24
25
26
27
28

(23)   Niles, E. T.; Roehling, J. D.; Yamagata, H.; Wise, A. J.; Spano, F. C.; Moulé, A. J.; Grey, J. K. J-Aggregate Behavior in Poly-3-Hexylthiophene Nanofibers. *J. Phys. Chem. Lett.* **2012**, *3* (2), 259–263.

29
30
31
32
33

(24)   Gao, J.; Kamps, A.; Park, S.-J.; Grey, J. K. Encapsulation of Poly(3-Hexylthiophene) J-Aggregate Nanofibers with an Amphiphilic Block Copolymer. *Langmuir* **2012**, *28* (47), 16401–16407.

34
35
36
37
38

(25)   Baghgar, M.; Labastide, J. A.; Bokel, F.; Hayward, R. C.; Barnes, M. D. Effect of Polymer Chain Folding on the Transition from H- to J-Aggregate Behavior in P3HT Nanofibers. *J. Phys. Chem. C* **2014**, *118* (4), 2229–2235.

39
40
41
42
43

(26)   Labastide, J. A.; Baghgar, M.; McKenna, A.; Barnes, M. D. Time- and Polarization-Resolved Photoluminescence Decay from Isolated Polythiophene (P3HT) Nanofibers. *J. Phys. Chem. C* **2012**, *116* (44), 23803–23811.

44
45
46
47

(27)   Podzorov, V. Organic Single Crystals: Addressing the Fundamentals of Organic Electronics. *MRS Bull.* **2013**, *38* (1), 15–24.

48
49
50

(28)   Reese, C.; Bao, Z. Organic Single Crystals: Tools for the Exploration of Charge Transport Phenomena in Organic Materials. *J. Mater. Chem.* **2006**, *16* (4), 329–333.

51
52
53
54
55

(29)   Hourani, W.; Rahimi, K.; Botiz, I.; Koch, F. P. V.; Reiter, G.; Lienerth, P.; Heiser, T.; Bubendorff, J.-L.; Simon, L. Anisotropic Charge Transport in Large Single Crystals of π-Conjugated Organic Molecules. *Nanoscale* **2014**, *6* (9), 4774–4780.

56
57
58
59
60

(30)   Reyes-Martinez, M. A.; Ramasubramaniam, A.; Briseno, A. L.; Crosby, A. J. The Intrinsic Mechanical Properties of Rubrene Single Crystals. *Adv. Mater.* **2012**, *24* (41),

5548–5552.

(31) Okada, Y.; Sakai, K.; Uemura, T.; Nakazawa, Y.; Takeya, J. Charge Transport and Hall Effect in Rubrene Single-Crystal Transistors under High Pressure. *Phys. Rev. B* **2011**, *84* (24), 245308.

(32) Liu, C.; Minari, T.; Lu, X.; Kumatani, A.; Takimiya, K.; Tsukagoshi, K. Solution-Processable Organic Single Crystals with Bandlike Transport in Field-Effect Transistors. *Adv. Mater.* **2011**, *23* (4), 523–526.

(33) Podzorov, V.; Menard, E.; Rogers, J.; Gershenson, M. Hall Effect in the Accumulation Layers on the Surface of Organic Semiconductors. *Phys. Rev. Lett.* **2005**, *95* (22), 226601.

(34) Minder, N. A.; Ono, S.; Chen, Z.; Facchetti, A.; Morpurgo, A. F. Band-like Electron Transport in Organic Transistors and Implication of the Molecular Structure for Performance Optimization. *Adv. Mater.* **2012**, *24* (4), 503–508.

(35) Tao, S.; Matsuzaki, H.; Uemura, H.; Yada, H.; Uemura, T.; Takeya, J.; Hasegawa, T.; Okamoto, H. Optical Pump-Probe Spectroscopy of Photocarriers in Rubrene Single Crystals. *Phys. Rev. B* **2011**, *83* (7), 75204.

(36) van der Poll, T. S.; Love, J. A.; Nguyen, T.-Q.; Bazan, G. C. Non-Basic High-Performance Molecules for Solution-Processed Organic Solar Cells. *Adv. Mater.* **2012**, *24* (27), 3646–3649.

(37) Irkhin, P.; Biaggio, I. Direct Imaging of Anisotropic Exciton Diffusion and Triplet Diffusion Length in Rubrene Single Crystals. *Phys. Rev. Lett.* **2011**, *107* (1), 17402.

(38) Labastide, J. A.; Thompson, H. B.; Marques, S. R.; Colella, N. S.; Briseno, A. L.; Barnes, M. D. Directional Charge Separation in Isolated Organic Semiconductor Crystalline Nanowires. *Nat. Commun.* **2016**, *7*, 10629.

(39) Hestand, N. J.; Spano, F. C. Interference between Coulombic and CT-Mediated Couplings in Molecular Aggregates: H- to J-Aggregate Transformation in Perylene-Based π-Stacks. *J. Chem. Phys.* **2015**, *143* (24), 244707.

(40) Hestand, N. J.; Tempelaar, R.; Knoester, J.; Jansen, T. L. C.; Spano, F. C. Exciton Mobility Control through Sub-Å Packing Modifications in Molecular Crystals. *Phys. Rev. B* **2015**, *91* (19), 195315.

(41) Pan, H.; Liu, P.; Li, Y.; Wu, Y.; Ong, B. S.; Zhu, S.; Xu, G. Unique Polymorphism of Oligothiophenes. *Adv. Mater.* **2007**, *19* (20), 3240–3243.

(42) Romang, A. H.; Watkins, J. J. Supercritical Fluids for the Fabrication of Semiconductor Devices: Emerging or Missed Opportunities? *Chem. Rev.* **2010**, *110* (1), 459–478.

(43)   Ferreira, V. R.; Gouveia, C. D.; Silva, C. A. da; Fernandes, A. N.; Grassi, M. T. Optimization of an Analytical Protocol for the Extraction, Fractionation and Determination of Aromatic and Aliphatic Hydrocarbons in Sediments. *J. Braz. Chem. Soc.* **2012**, *23* (8), 1460–1468.

(44)   Pretorius, N. O.; Willemse, C. M.; de Villiers, A.; Pasch, H. Combined Size Exclusion Chromatography, Supercritical Fluid Chromatography and Electrospray Ionization Mass Spectrometry for the Analysis of Complex Aliphatic Polyesters. *J. Chromatogr. A* **2014**, *1330*, 74–81.

(45)   Zhang, L.; Colella, N. S.; Liu, F.; Trahan, S.; Baral, J. K.; Winter, H. H.; Mannsfeld, S. C. B.; Briseno, A. L. Synthesis, Electronic Structure, Molecular Packing/morphology Evolution, and Carrier Mobilities of Pure Oligo-/poly(alkylthiophenes). *J. Am. Chem. Soc.* **2013**, *135* (2), 844–854.

(46)   Hestand, N. J.; Yamagata, H.; Xu, B.; Sun, D.; Zhong, Y.; Harutyunyan, A. R.; Chen, G.; Dai, H.-L.; Rao, Y.; Spano, F. C. Polarized Absorption in Crystalline Pentacene: Theory vs Experiment. *J. Phys. Chem. C* **2015**, *119* (38), 22137–22147.

(47)   Yamagata, H.; Maxwell, D. S.; Fan, J.; Kittilstved, K. R.; Briseno, A. L.; Barnes, M. D.; Spano, F. C. HJ-Aggregate Behavior of Crystalline 7,8,15,16-Tetraazaterrylene: Introducing a New Design Paradigm for Organic Materials. *J. Phys. Chem. C* **2014**, *118* (49), 28842–28854.

(48)   Yamagata, H.; Spano, F. C. Interplay between Intrachain and Interchain Interactions in Semiconducting Polymer Assemblies: The HJ-Aggregate Model. *J. Chem. Phys.* **2012**, *136* (18), 184901.

(49)   Baghgar, M.; Barnes, M. D. Work Function Modification in P3HT H/J Aggregate Nanostructures Revealed by Kelvin Probe Force Microscopy and Photoluminescence Imaging. *ACS Nano* **2015**, *9* (7), 7105–7112.

(50)   Provencher, F.; Bérubé, N.; Parker, A. W.; Greetham, G. M.; Towrie, M.; Hellmann, C.; Côté, M.; Stingelin, N.; Silva, C.; Hayes, S. C. Direct Observation of Ultrafast Long-Range Charge Separation at Polymer–fullerene Heterojunctions. *Nat. Commun.* **2014**, *5*, 4288.

(51)   Paquin, F.; Latini, G.; Sakowicz, M.; Karsenti, P.-L.; Wang, L.; Beljonne, D.; Stingelin, N.; Silva, C. Charge Separation in Semicrystalline Polymeric Semiconductors by Photoexcitation: Is the Mechanism Intrinsic or Extrinsic? *Phys. Rev. Lett.* **2011**, *106* (19), 197401.

1
2
3
4
5
6
7
8
9
10
11
12
13
14
15
16
17
18
19
20
21
22
23
24
25
26
27
28
29
30
31
32
33
34
35
36
37
38
39
40
41
42
43
44
45
46
47
48
49
50
51
52
53
54
55
56
57
58
59
60

TOC